Effects of Space Plasma on an Oxide Coating of Spacecraft's Surface Materials

Afaf M. Abd El-Hameed[1], Yehia A. Abdel-Aziz[1], M. I. Ismail[2]

Laila Abo hashim[3], and Anna Gregorio[4]

[1]National Research Institute of Astronomy and Geophysics, NRIAG, 11421, Cairo, Egypt
[2]Faculty of Engineering, Zagazig University, Egypt
[3]Faculty of Engineering, beni suef University, Egypt
[4]Department of Physics - University of Trieste, Italy

Abstract

The current work concerns studying of charging/discharging processes and properties of the materials for spacecraft' surfaces under the effects of simulated low Earth orbit (LEO) plasma environment at National Space Plasma Interaction Unit (N-SPI-U), NRIAG - Egypt. Experimental studies are performed to simulate the electrical breakdown of the anodizing oxide film coatings of aluminum substrate. Experimental tests are carried out to investigate the charging and discharging phenomena of anodized aluminum surface exposed to simulated LEO-plasma with different conditions and properties. The anodized aluminum samples (AAS) are prepared using the electrochemical technique. Two samples of anodic coatings Al_2O_3 are formed on the aluminum plates and produced with different film thicknesses of 13 μm and 25 μm, to check and understand the occurrence of charging and discharging phenomena. Penning plasma source is used to generate plasma using Argon (Ar) gas flowing through the evacuated chamber. Negatively-biased voltage is applied on the samples, and the peak current and voltage waveform associated with charging and discharging processes are discussed. The structural characteristics before and after plasma exposure are investigated through the morphology and optical analyses of the samples. The obtained results confirm the effects of space plasma on the spacecraft'surface characteristics with the variation in the anodic oxide films properties as well as the micro-crystalline structure over the surface.

Key words: Anodized Aluminum Samples (ASS); Anodic film coatings; Ar plasma; Bias voltage; Charging/Discharging; Structural characteristics; Morphology and Optical Analyses.

1. Introduction

The environmental effects played an important role in determining the spacecraft's reliability and lifetime. Spacecraft surfaces are exposed to energetic and reactive particles, such as electrons, ions, protons and oxygen atoms and ultraviolet light, including particles exhausted from plasma thrusters, during space missions (Teichman, 1989, Masahito, et al., 2010, and Arifur et al., 2013). In space plasma environment, through the electrostatic interactions between the surface materials and the ambient plasma, such as negative or positive sheath creation, the charging and discharging phenomena are frequently observed (Hillard and Ferguson, 1995, Zhang, et al., 1997, Mengu Cho, 2007, Akitoshi, et al., 2014, Suryakant, et al., 2014, and Suryakant, et al., 2016). In LEO-plasma, the neutral particles as well as charged particles around spacecraft played an important role in expansion of arc plasma causing the arcing characteristics. Large arcs may locally disrupt the surface, interrupt power for a short time, and produce prompt contamination. Therefore, the environmental factors cause changes of chemical structures of spacecraft materials and their optical and electrical properties (Tribble, et al., 1996, and Tahara, et al., 1997). For thermal properties, some of the insulating paints are often used to control the temperature of the surfaces of LEO spacecraft (Robinson and Whittlesey, 1980, and Leung, 1989). On the other hand, the aluminum and its alloys is considered to be the common materials used for spacecraft structures and surfaces because it is cheap, lightweight and easy to anodize (Hillard et al 2000, Hillard, and Vayner 2000 Todd et al 2001, and Tyler, et al., 2006). The weakness and failure of aluminum properties can be reduced by anodization. An anodized aluminum is one of the more interested materials in using of external spacecraft surfaces. The optical properties of the anodizing layer applied on the aluminum can produce a surface having thermal control properties. The insulating properties of this material may cause the designers to use it in high-voltage space power systems. The operation of the higher voltage spacecraft may cause degradation of spacecraft surfaces and the anodized aluminum coatings through the discharging and arcs depending on plasma condition and spacecraft capacitance (Ferguson, 1991, Hillard and Vayner, 2000, Takahisa, 2003, Abdel-Aziz, et al., 2013, Fukuda, et al., 2017). International Space Station (ISS) is a good example for the anodized aluminum components utilized in many key areas. Dielectric breakdown and arc generation can lead to damage the anodized surface with the production of significant electromagnetic interference (Galofaro, et al.,

1999, Hillard, and Vayner, 2000, Hillard, et al., 2000, Todd et al., 2001, and Black Tyler, et al., 2006). In case of spacecraft with the aluminum surface structure, these arrays are electrically connected with the aluminum structure. Because of the mobility of ions of plasma is much less than the electrons, these arrays are floating with negative potentials in order to reach the current balance with the electrons. This sequentially leads the structure to have a negative potential respecting the ambient plasma. In the anodic layer coating applying on the aluminum, the surface becomes a dielectric surface, and appears to be a capacitor. In this capacitor, the dielectric layer is enclosed between the two conducting surfaces (the aluminum and the plasma). For the higher values of bias voltage, the discharging and arcs are occurred depending on the plasma conditions and spacecraft capacitance. These arcs may cause damage of the dielectric surface (Jongeward and Katz, 1998, Hillard and Vayner, 2000, Hillard et al., 2000, Tyler, et al., 2006, and Abd El-Hameed et al., 2015).

In this work, we focus on LEO- plasma induced discharging and electrical breakdown processes on the surface of an anodized aluminum coating. Ground-based simulations are performed to investigate the charging and discharging characteristics on samples of anodized aluminum plates with different film thicknesses of 13 μm and 25 μm, immersed in Ar-plasma environment. Morphology, surface properties as well as sample characteristics are analyzed under the effects of plasma exposure.

2. Anodic Oxide Film Formation

Anodizing process is an electrochemical technique that converts the metal surface into an oxide. Therefore, in National Space Plasma Interactions Unit (N-SPI-U) at NRIAG institute, thin film anodic oxide coating is produced on a sample of an aluminum plate and prepared using electrochemical cell with aqueous solution of sulfuric acid (15 wt % H_2SO_4, 22°C, 12 V) at a current density (2 A/dm^2). In this method, two plates of stainless steel (cathode) and aluminum to be anodized (anode) are immersed in the solution. The time period for the anodic process is chosen to be 60 minutes followed by a hot water used to seal the sample for about 15 minutes (Abd El-Hameed et al, 2017). The anodic film is formed with thickness of about 25 μm. The same procedures are applied using different values of the current density and time period to prepare a considerably thin coated film. In this case, an anodic coated film of thickness 13 μm is formed on another aluminum plate sample. These thicknesses are measured using a digital

electronic coating thickness gage. These samples are performed to investigate the discharging and arc, peak current and voltage waveforms in the experimental study.

Fig. 1a shows the macroscopic image for a selected area with dimensions (1 cm x 1 cm) of the anodic sample surface of thickness 25 μm. This image is taken using the CCD camera with (4 x 0.1) lens (Ts View 5MP, with the pixel size 2592H x 1944V) connected with an optical microscope. This image is enlargement with the optical microscope (of lenses 4X) and analyzed using the image processing program specifically Maxim-DL astronomical software as shown in Fig. 1b. This software is used as photometrical technique for the analysis of the object. The figure describes the three dimensional spatial distribution of the anodic oxide surface concentration. The X and X axes illustrate the selected area of the sample (pixel size), and with unit of pixels, whereas, the Z axis clarifies the particles density distributed on the surface. The difference in colors represents the luminance intensity due to the variation of the density and particles concentration on the surface. This is cleared as changeable on the brightness and luminance distribution on the sample surface. The images of these figures show the roughness and fluctuation in the density of the particle concentration distributed on the surface.

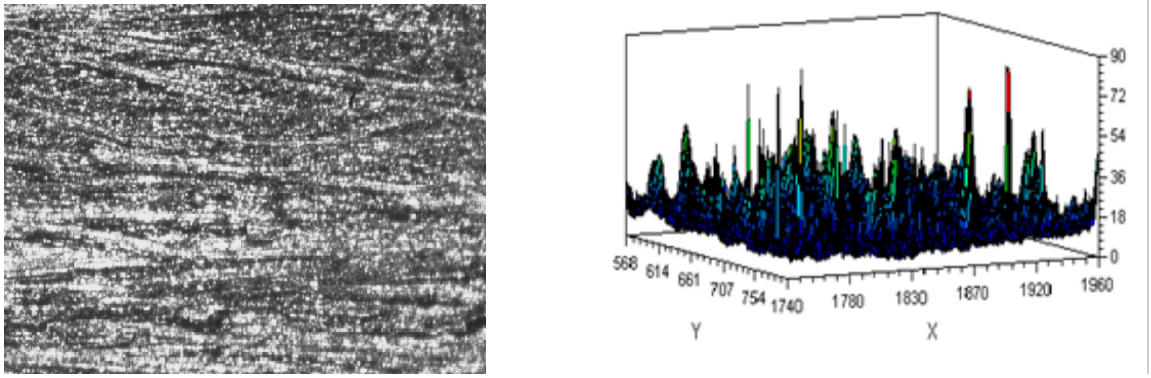

(a) (b)

Fig.1. (a) CCD image of a selected area with dimensions of (640 x 480) pixels of the surface, before plasma exposure, and (b) the spatial distribution for the image of (a) with a relative mean value of pixels (intensity I = 155).

The optical properties of the used samples are analyzed through the measurements of the absorption and reflection spectra. Accordingly, the following figures illustrate the properties of the aluminum sample without and with the anodic oxide coating of the sample surface.

Figs. 2 describe the UV normalized absorption spectra of the aluminum surface (Al) and the anodic oxide surface (Al_2O_3) represented as 2a and 2b respectively. The absorbance here

quantifies how much of the incident light is absorbed by the surface of the sample. The two surfaces show great absorption in the UV region than that of the visible region. A well-defined sharp and strong absorbance peak is located and shifted toward the short wavelength about 200 nm. This indicates the narrow particle size distribution. Therefore, the absorbance has a great value in the ultra-violet region and decreases sharply with increasing the wavelength, which becomes almost constant with the low values towards the visible region. The low absorption values are obtained in case of the oxide surface (Al_2O_3) due to porosity, deformation, and formation of non-**chopped** surface leading to creation the non-homogeneous surface.

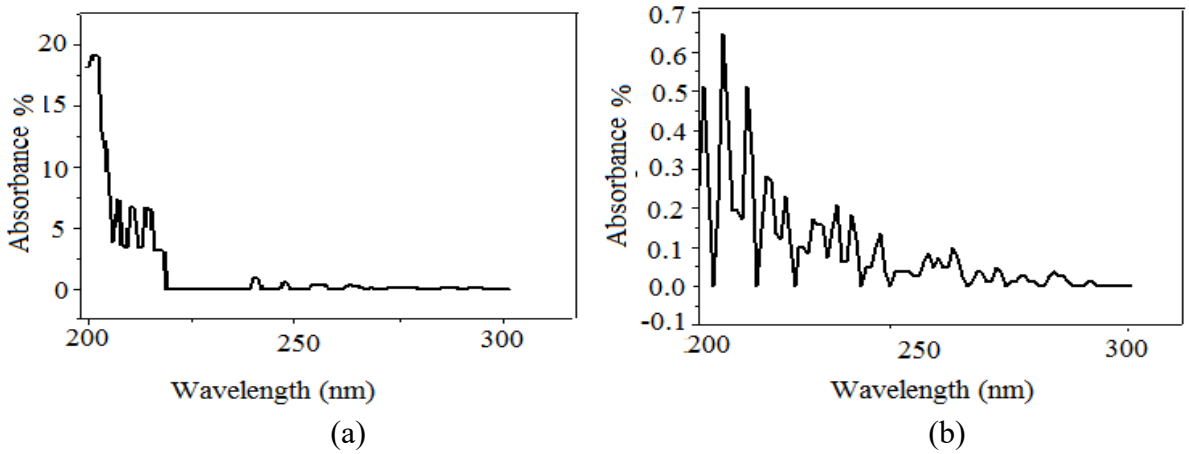

Fig.2. UV absorption spectra of the (a) Al surface and (b) Al_2O_3 film before plasma effect

Fig. 3 demonstrates the variation of reflectance spectra with the wavelengths for the aluminum (red line) and oxide film Al_2O_3 (blue line) surfaces. The figure shows that, in the UV-region, the results verify the decreasing in the reflectance to lower values and gradually increase with the higher wavelengths. It is noticed from the figure that, in the anodized oxide film Al_2O_3, the curve is stepped at about 1000 nm. This is probably because of the brightness and shiny surface due to the formation of deep porous, and the surface here likes as aluminum layer in this point. Moreover, the anodic oxide thin film provides a low level of reflectance than that obtained in the aluminum surface. This behavior clarifies that, the grain size and consequently the increasing in surface roughness can lead the decreasing in specular reflectance. This confirm the shiny and homogeneity of aluminum surface can lead to be more reflectance than in case of the coated surface, in which the porous and fluctuations in the crystalline structure can cause shadow and dim surface. In addition, the reflectance of aluminum is generally increased with the increasing in thickness of the aluminum layer.

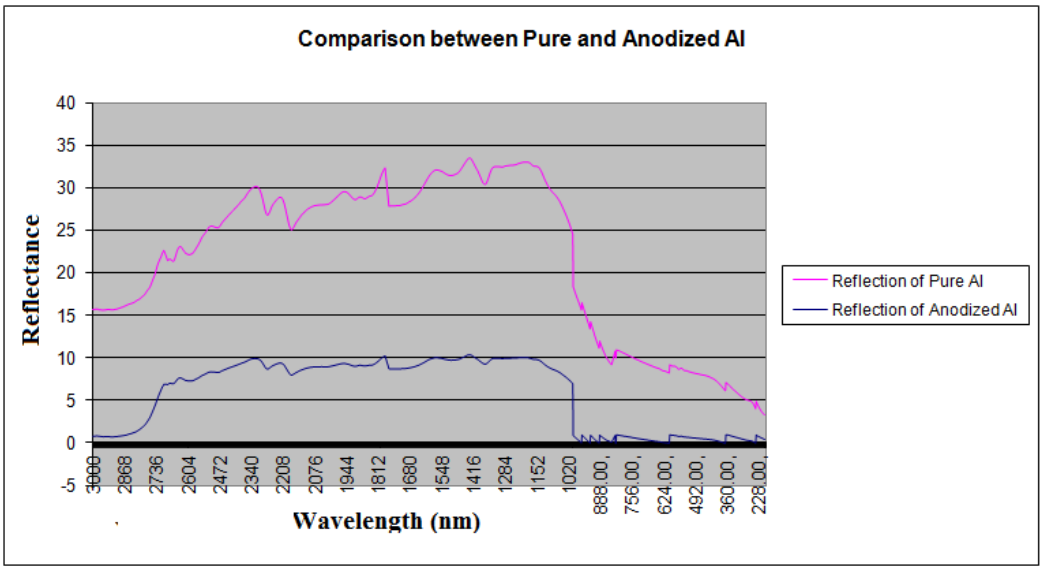

Fig.3. UV/Vis/NIR reflection spectra of Al (red) and Al_2O_3 film (blue) before plasma effect

To analyze the aluminum surface sample before and after the anodic process, Fourier Transform Infrared Spectroscopy (FTIR) analysis is used. The FTIR analysis provides the amount of the infrared light (IR) absorbed by the material at different frequencies. The infrared light is used to scan test samples and observe the chemical properties. The Processes of this test is into two steps. First, the sample is placed in FTIR spectrometer. The spectrometer directs beams of IR at the sample and measures how much of the beam and at which frequencies the sample absorbs the infrared light. In the second step, the reference database houses thousands of spectra, so samples can be identified. The FTIR spectrometer simultaneously collects high spectral resolution data over a wide spectral range.

Therefore, Fig. 4 shows the FTIR absorption spectra of the aluminum (Al) sample surface. In this figure, the peaks are roughly located around the same maximum absorption value at all frequency bands because of the shiny, glossy, and a considerably homogeneous aluminum surface. On the other hand, for the anodic film Al_2O_3, this behavior is different as illustrated in Fig.5. In this figure, due to the oxide layer, the peaks are observed with higher absorbance values at frequency bands up to 412.671 $cm^{-1}$and 512.972 cm^{-1}, and tended to be approximately the same with small values for all other frequency bands.

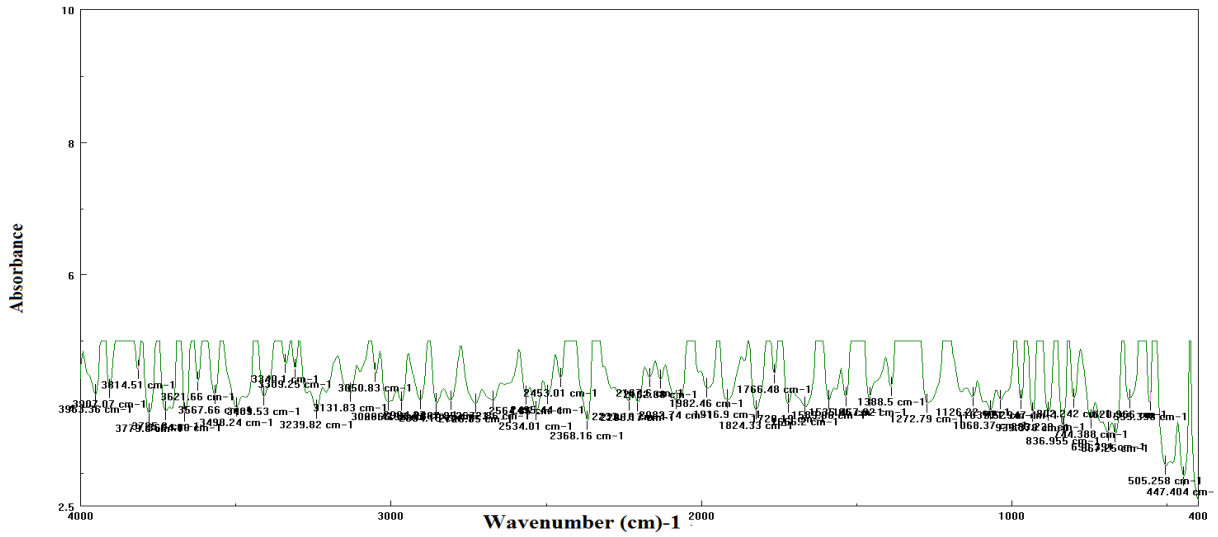

Fig.4. FTIR absorption spectra of the Aluminum (Al) surface sample without anodic process

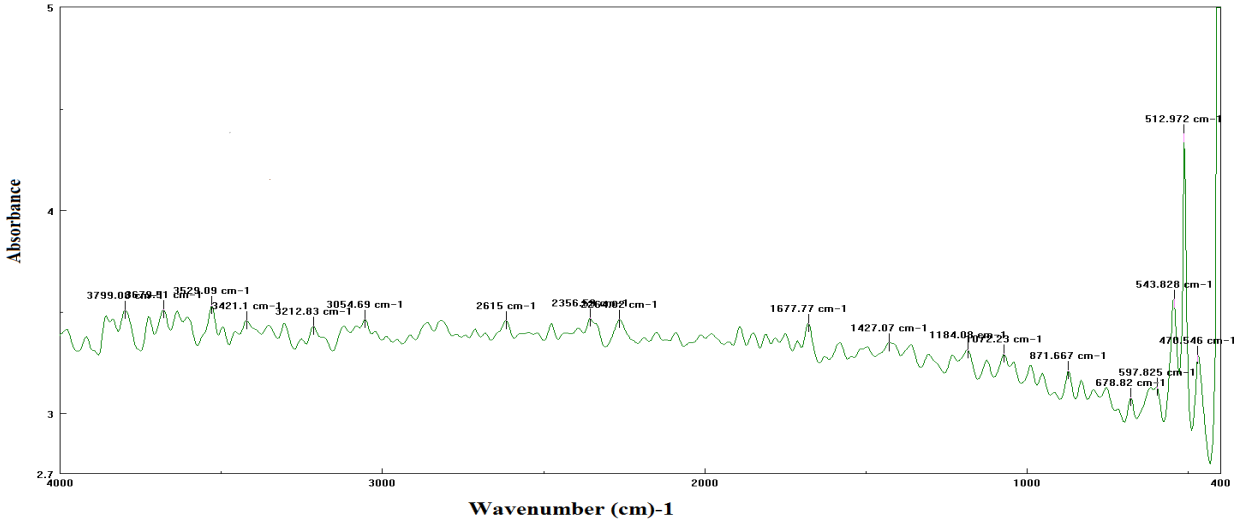

Fig.5. FTIR absorption spectra of the anodic oxide surface Al_2O_3

3. Experimental Study

In the present tests, ground-based vacuum facilities have been performed at (N-SPI-U) unit to simulate LEO plasma environment. In the laboratory, a cylindrical vacuum chamber is used and pumped to pressure of 10^{-5} torrs. Penning plasma source is used to generate plasma from argon gas flowing through the chamber test. Electrons are emitted from a filament and generate electrical discharge in the glow arc regime. This discharge generates plasma between

the cathode and surrounding anode. The properties of the generated plasma are measured using the Langmuir probe. From the data obtained through the probe, the electron temperature and plasma density are calculated. Table 1 explains the plasma properties and test conditions estimated and calculated through the flowing gas pressure about (P_{Ar} = 0.6 mbar). The operating point of the filament of the source is 16 A, and the potential difference between the filament and the surrounding anode is 750 V. More detailed explanation of the employment procedure for the calculation of the plasma parameters has been clarified in the work of (Abdel-Aziz, et al, 2013).

Test conditions	Ar-plasma parameters
Chamber pressure ($P = 10^{-5}$ torr)	Electron density ($n_e = 0.5 \times 10^6$ cm^{-3})
Anode potential (750 V)	Plasma temperature ($T_e = 0.79$ eV)
Filament condition (16A at 5V)	Ion velocity = 700 m/S
Anode current (0.5 A)	Debye length ($\lambda = 0.7$ mm)
	Flowing gas pressure ($P_{Ar} = 0.6$ mbar)
Degree of ionization	10^{-4}

Table1. Test conditions and plasma parameters

The generated Ar plasma is applied on the two samples of two different coated thicknesses formed in the laboratory. These samples are identified for coated thickness of 13 μm as sample (I), and for coated thickness of 25 μm as sample (II). These thicknesses can allow the occurrence of the discharging and arcing processes at lower bias voltages (Tyler, et al., 2006). The experimental procedures are carried out for the two samples taken with the same dimensions (5cm x 5cm). The experiments have done into two different steps. In every step, the sample plate is mounted on a holder, which is located inside and near the center point of the vessel chamber. The back of the plate beside to the edges are covered with kapton and the front side only is interacted with the plasma. Outside the chamber, the sample is connected with an electric circuit contains resistance and capacitor. Moreover, Different tools such as current probe and oscilloscope are considered to investigate the plasma and sample characteristics. Test facilities and schematic of the experimental configuration is given in Fig.6.

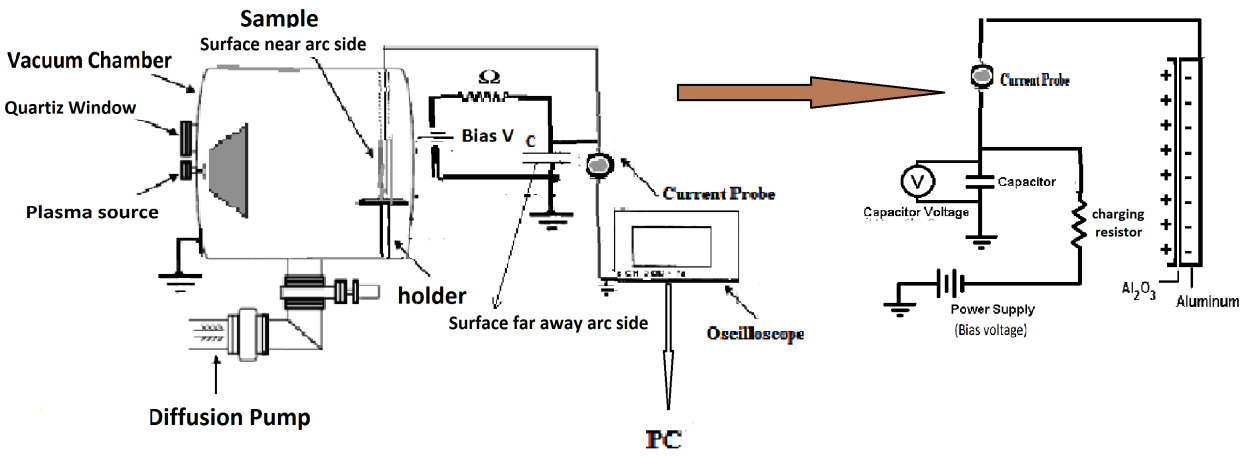

Fig.6. Basic schematic of the experimental configuration and diagram for the circuit of the sample

The anodized samples are tested for various time duration at a negatively biased voltage (-70V) to identify the waveform of the occurrence of peak current and arc event. This voltage may be suitable for the thickness of the anodized surface with a sufficient dielectric strength. Different external capacitances and values of added resistance are studied to help characterize the current levels and time durations associated with the arc process.

4. Results and Discussion

4.1. Discharging and current behavior

4.1.1 Sample (I)

In the laboratory experiments, the sample (I) is tested under the effects of plasma exposure. To simulate spacecraft capacitance, an external capacitor of a roughly (24 μF) is installed and connected between the sample and the vacuum chamber, i.e. the ground. This capacitor is charged with the negative voltages of power supply to simulate the floating negative potential of spacecraft surface. The anodic surface of the sample is considered as the spacecraft surface near the arc side, while the capacitor in the sample circuit simulates the surface far away the arc side. A resistance of 5 ohms is applied on the experiment. Fig x clarifies the voltage waveform and peak current observed during the discharging and arc process. The figure is plotted for the data taken from a current probe connected in the circuit. This probe is connected with the oscilloscope, in which the data are recorded and described the voltage waveform during

the discharging and arc processes. Typical waveforms of the current trace through the discharging process. The trigger arc is observed with the high peak current and after small time duration.

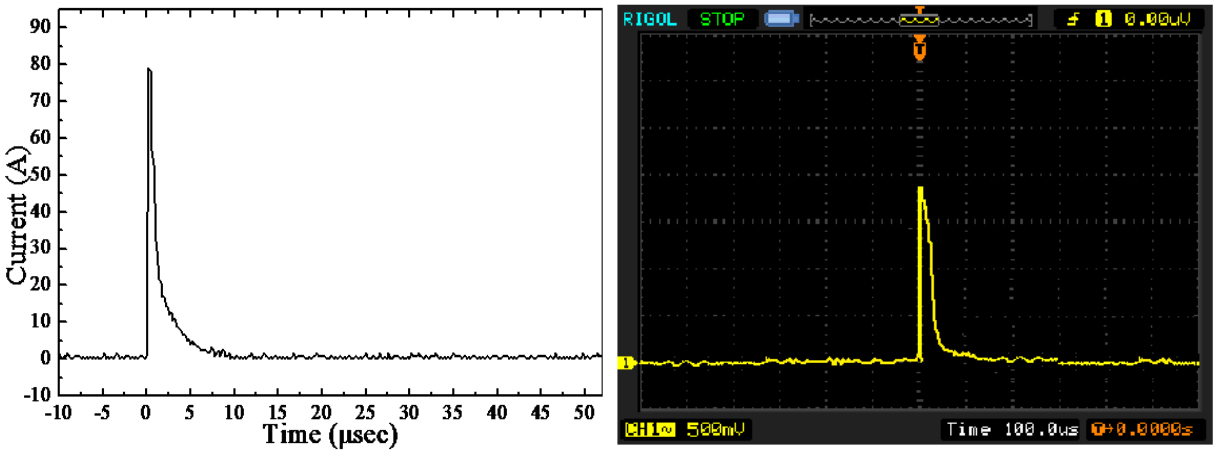

Fig x Current and voltage waveform of the sample (I) with r esistance (5 Ohm)

4.1.2 Sample (II)

In this case, an external capacitor of (12 µF) is used and connected in the circuit. Two resistance values of 5 ohms and 500 ohms are applied on the experiment. Fig. (7a and 7b) illustrate the discharge current behavior shown as figure 7a, and the voltage waveform as figure 7b of the sample (II) and with the applying resistance of 5 ohms in the circuit. The current flow is recorded through an oscilloscope with the total duration of (50 µ sec). Whereas, Fig. (8a and 8b) are plotted for the recorded data with the applied resistance of 500 ohms and using the same capacitor (12 µF). The observed currents in Figs. 7 and 8 are corresponded to the discharging initiating on an anodized plate. The two figures clarify the current behaviors and traces, which are reached to a peak value before tends to be lower due to the discharging process. The waveforms shown in the figures clarify the time dependence of the current during an arc event. A typical arcing sequence has the following regions; the region in which the arc is initiated and the current increases to a peak value and the current remains near the peak value for some time. The other one is the region for the decreasing in current with a roughly exponential decay, in which the current is space-charge limited. The signal traces of the two figures are simultaneously triggered, and display what is sensed by the probe. The oscillations observed in the probe traces are due to the quasi-neutral plasma cloud.

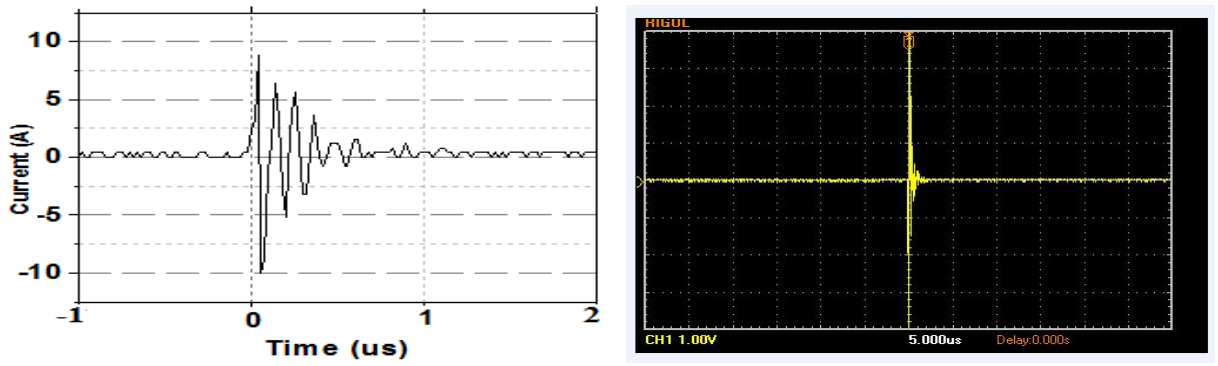

(a) (b)

Fig.7. (a) Peak arc current and (b) voltage waveform on the sample (II) with resistance (5 Ohm)

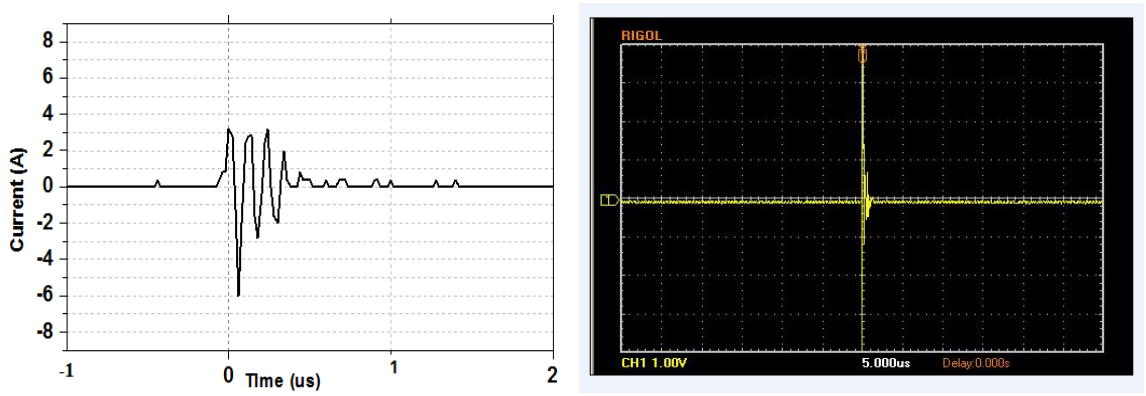

(a) (b)

Fig.8. (a) Peak arc current and (b) voltage waveform on the sample (II) with resistance (500 Ohm)

Fig. 9 clarifies the average values of peaks the current with different resistances 5ohms, 50 ohms, and 500 ohms. The data are plotted for all current traces within the total pulse duration, and with 20 arcs for each resistance. The error bars on the graph represents the standard deviation of the points in the test data. It is noticed that the peak current is gradually decreased with increasing applied resistance. The figure confirms the high currents and peaks and their inversely relations for each resistance are obtained over all traces.

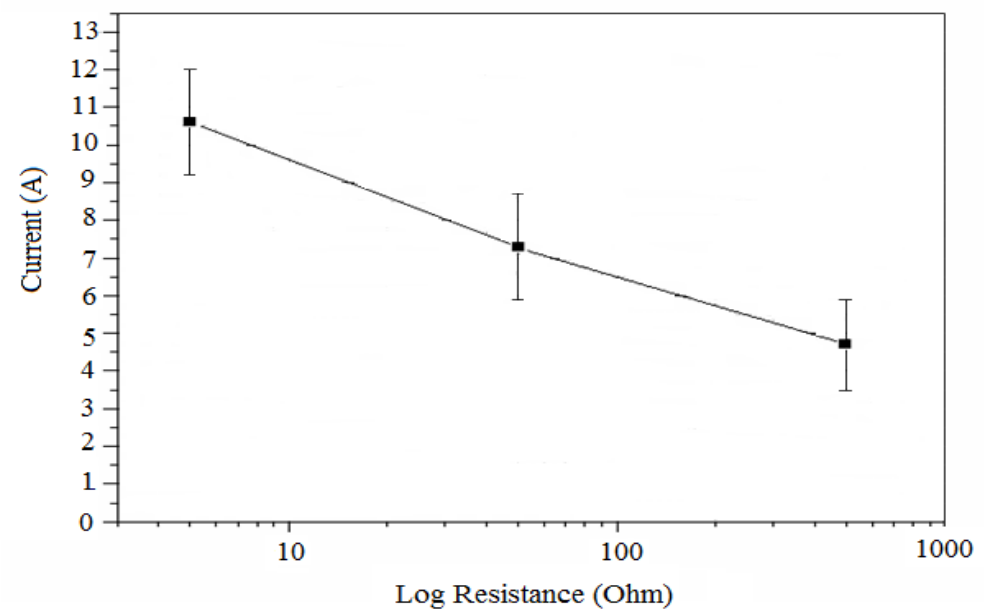

Fig. 9 The average peak current versus resistance

The above results can be concluded as;

- Higher peak currents are obtained with the lower thickness value.
- The increasing in the applied capacitor leads to increase the peak current.
- The increasing in the resistance values lead to decrease the peak current.

These results are comparable with the results obtained from the experimental studies of many authors as the works of (Tyler, et al., 2006), (Galofaro, et al., 1998), (Hirokazu Tahara, et al, 2006) and (Galofaro, et al., 1999).

4.2. Structural and optical characteristics

To investigate and verify the variation on the physical properties of the samples under the effects of plasma exposure, sample (II) is considered, as an example, to check and analyze the optical characteristics and crystalline structures.

4.2.1 Optical properties

Atomic concentrations of "Al" and "O" of the oxide film Al_2O_3 sample before and after plasma effect are checked and analyzed through the Electron Dispersion X-Ray Spectroscopy (EDS or EDX). EDS is a chemical microanalysis technique used to detect the x-rays emitted from the sample during bombardment by an electron beam. This technique is carried out to

characterize the elemental composition of the analyzed volume. The EDS analysis can give relative quantification from the atomic concentrations. The instrumentation and initial data conditions for the analysis are given in table (2). The factor PHA mode represents the resolution of the instrument, and T3 is the high level for the resolution. Acc. Voltage is the acceleration voltage and takes the ranging values between 15-20 KV. This range is good for EDS analysis, while for high resolution imaging of materials in secondary electrons, acceleration voltage of 25-30 kV is more appropriate. The real time is the clock time and divided into live time and dead time. The live time is the time when the detector is alive and able to receive an x-ray event (i.e. the time when it is doing nothing) and the dead time is when the detector or preamplifier is unable to accept a pulse because it is busy processing or rejecting an event. The analyses are carried out using the "ZAF" method standardless quantitative analysis, in which the atomic number correction Z, the absorption correction A, and the fluorescence correction F are evaluated. Filtered Least-Squares Peak Fitting method with different experimentally measured spectra as peak references is used to estimate the fitting coefficient.

Acquisition Parameter	Values
Instrument	6510(LA)
Acc. Voltage	30.0 KV
Probe Current	1 nA
PHA mode	T3
Real Time	662.30 sec
Live Time	50.00 sec
Dead Time	92 %
Energy Range	0 - 20 KeV
Counting rate	48115 cps
Fitting Coefficient	0.4354

Table2. Parameters and conditions used for EDS analysis

The quantitative analyses for the sample before and after plasma effects are shown in tables (3) and (4) respectively. The results of the quantification of elements are presented in the mass % and atoms %. The EDS measurements are taken for different points on the surface and their

mean value is considered as the composition of sample. The results of the analyses are shown in Fig (10). From the data analysis, the presence of the elements “Al” and “O” is detected. The analyses provide the total percentage of the element presented in the selected sample. The systematic error is determined from the five repeated measurements of the five samples (1 spectra for each) to get the systematic error.

Element	(keV)	Mass%	Error%	Mol%	Compound	Mass%	K
O	----	47.09	----	---	Al_2O_3	----	
Al K	1.486	52.91	1.01	100.00		100.00	16.00
Total		100.00		100.00		100.00	16.00

Table (3): Quantitative analysis for the sample before plasma effect

The symbol “Kα” presented in Fig (10) describes the K line for the energy levels. The symbols “OKα, and Al Kα” represent the atomic concentration of oxygen”O” and aluminum “Al” at the line K-shell in the energy levels.

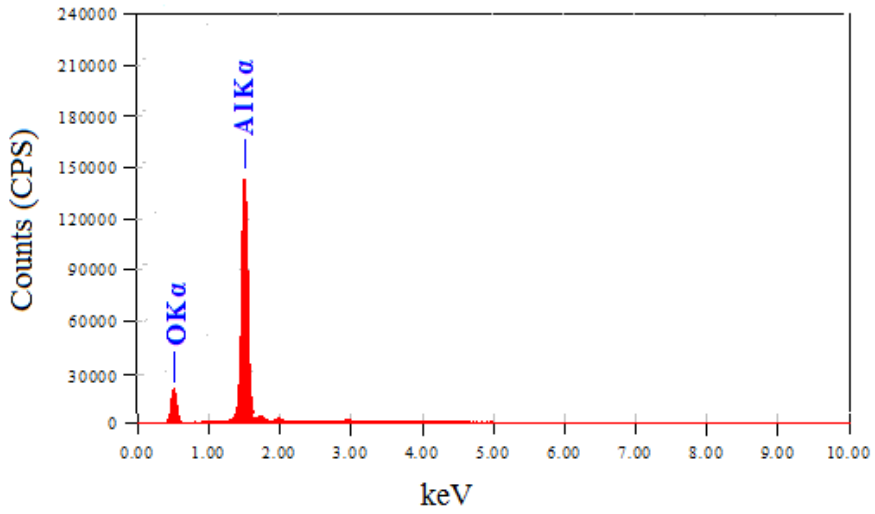

Fig.10. EDS analysis for the Al_2O_3 sample without plasma effect

Figure 11 clarifies the energy of the element concentrations released due to plasma exposure. The figure illustrates the decrease of the values for the elements of the anodic surface due to

plasma effects. It is noticed that, the oxide layer is going to remove due to damaging the anodizing after plasma exposure. On the other hand, another element such as molybdenum "Mo" atoms is appeared. This indicates the variation of surface film crystalline structure in which the appearance of the Mo element is considered as the impurity embedded in the manufacture of the aluminum plate itself. This element is a very low level impurity in aluminum and has been used as a grain refiner. The symbols "Mo Mα" and "Mo Lα" describe the atomic concentration of the element "Mo" in the energy levels of lines M-shell and L-shell respectively. The observed different elements have different surface binding energies which have a significant effect on the propagation of the collision cascade.

Element	(keV)	Mass%	Error%	Atom%	Mass%	K lines
Mo L	2.293	19.69	4.39	5.20		17.0129
O K	0.525	30.20	1.62	47.79		18.1140
Al K	1.486	50.1	0.36	47.01		64.8731
Total		100.00		100.00	99.99	100.00

Table (4): Quantitative analysis for the sample after plasma effect

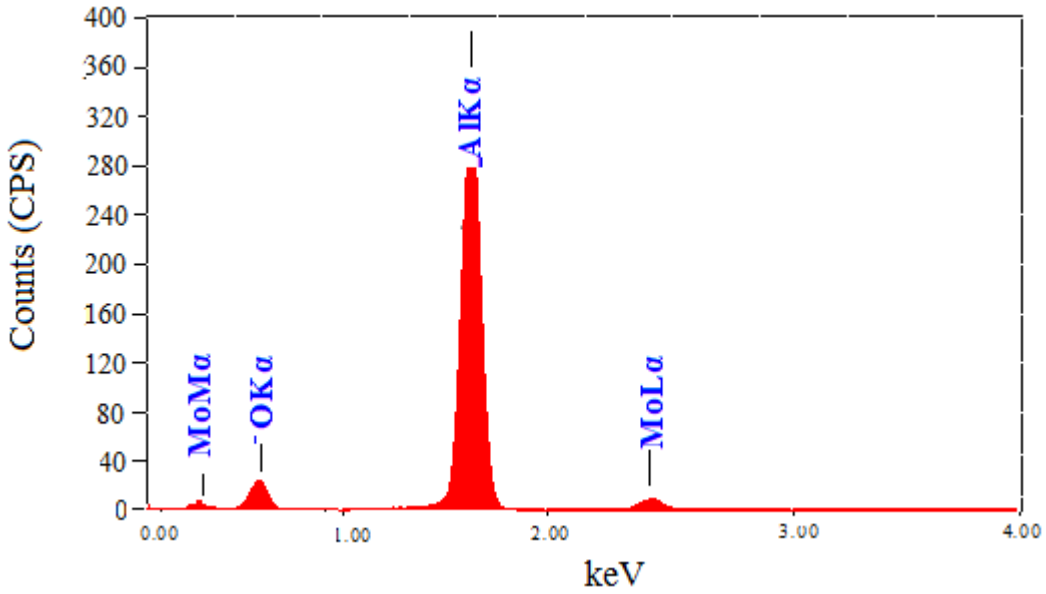

Fig.11. EDS analysis for the Al_2O_3 sample after plasma effect

Fig. 12 illustrates the UV/Vis/NIR reflectance spectra of the oxide film Al_2O_3 surface after plasma exposure. The figure shows approximately the same behavior obtained in Fig.3. The figure clarifies the increasing of reflection at all band regions of the wavelength. This behavior is probably due to;

Variation in the micro-crystalline structure and the different surface binding energies for the elements of the sample,

Occurrence of sputter and etching on the surface,

Surface is get rid and eliminate of outstanding impurities,

Surface becomes more polished and gloss.

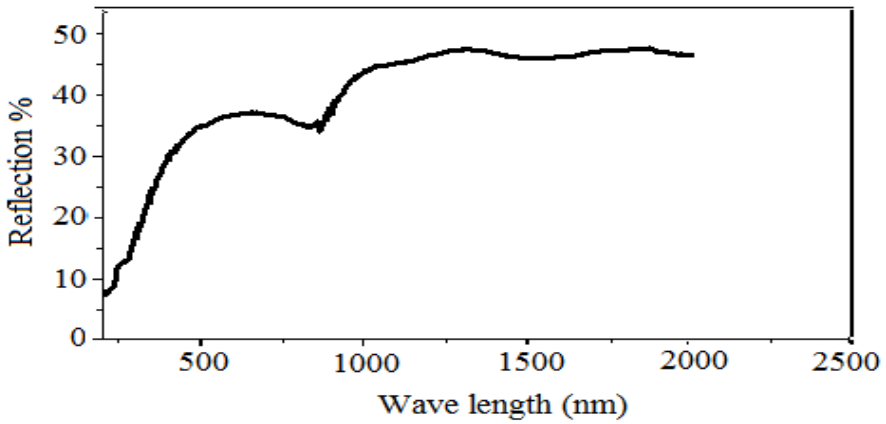

Fig.12. UV/Vis/NIR reflection spectra of Al2O3 surface after plasma effect

4.2.2 Morphological Analysis

To assure the plasma effects on the surface roughness and particles distribution, Fig. (13a and 13b) describe the macroscopic image taken with the same CCD camera and optical microscope considered in figure (2a, 2b) and for the same selected sample and conditions. The figures show that, the density and particles concentration become less roughness with more homogeneity, and the surface becomes uniform with less deformation and porosity. This can explain the thermal energy of the plasma causes the collision of the surface particles leading to the rearrange and redistributed of these particles on the surface, which is observed with low impurities and more polished and glossy.

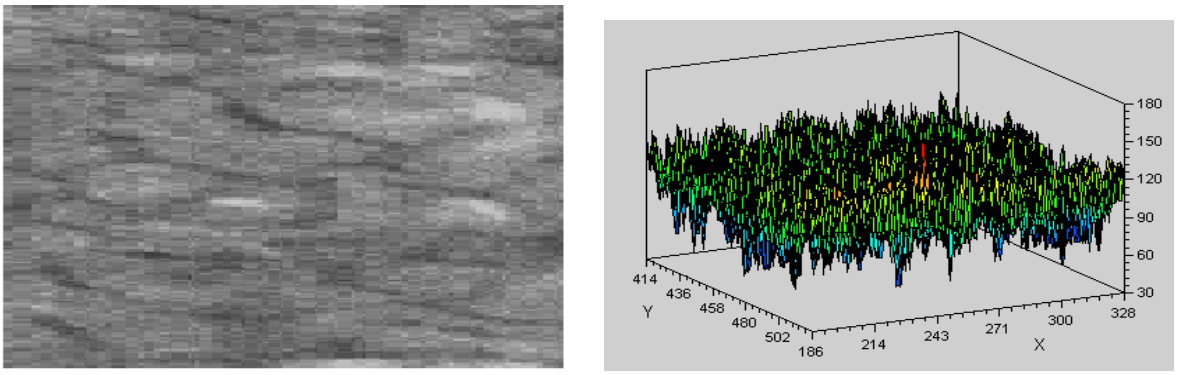

Fig. 13 CCD image for the same selected area (a) taken from the surface after plasma exposure, and (b) the spatial distribution for this image

More clearly, to confirm the variation of the anodic oxide film characteristics, Scanning Electron Microscope (SEM) is used to analyze the sample surface before and after plasma effects. Fig (14a, 14b) show the SEM images of the anodic oxide surface Al_2O_3 before and after plasma effect respectively. The morphology scales are taken to illustrate the microstructure of the surface. Fig. 14a shows that, the particles are dispersed revealing fracture and crack surface, also an inhomogeneous layer coating is observed with the grain size and therefore surface roughness increases. In addition, some holes indicating porosity is present and the micrometer crystallites distributed less uniformly over the surface. Fig. 14b confirms the effecting plasma on the crystallites which become more uniformly over the surface. Few cracks and porosity are observable with a quite different microstructure in comparison with Fig. 14a. The crystallite sizes become small scales with low surface roughness, leading to the change of the surface to be gloss.

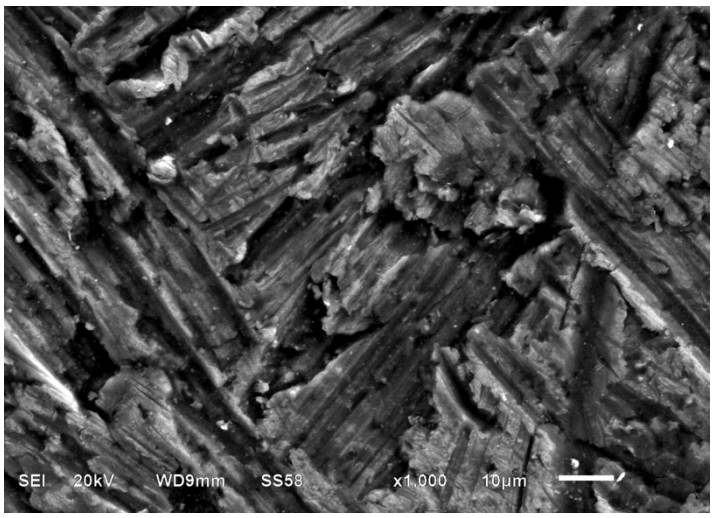

(a)

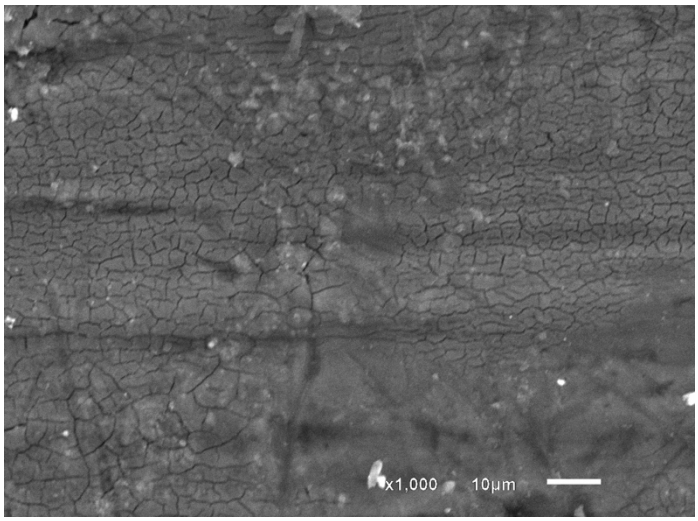

(b)

Fig.14 SEM images for the anodized surface Al_2O_3 (a) before plasma effect and (b) after plasma effect

5. Conclusion

At National Space Plasma Interaction Unit (N-SPI-U), NRIAG - Egypt, we have investigated the charging and discharging phenomena of anodized aluminum surface exposed to simulated LEO-plasma with different conditions and properties. The anodized aluminum samples are carried out in the laboratory using the electrochemical technique. We have tested two different anodic oxide films formed on the aluminum plates with thicknesses of 13 μm and 25 μm. The results checked which thickness can be applicable and meet the required coated film to mitigate the discharging and arcing processes. The results discussed and described the variation of the anodic oxide film coating characteristics of the aluminum plates under the effects of simulated LEO- plasma. We examined the properties and structural characteristics of the sample of the coated thickness of 25 μm, as example, before and after plasma exposure. Morphological analyses have shown a significant contribution of space plasma in the variation of the crystalline structure and sample characteristics. In addition results confirm the variation of optical properties and the micro-crystalline structure over the surface of the anodic oxide film as well. The obtained results can be helpful to understand the behavior of charging and floating potential throughout spacecraft and may be useful in attempt to limit the potential of spacecraft systems with respect to the plasma in order to mitigate arcs, or to at least to limit the amount of

connected capacitance available to potential arc sites. Finally this kind of study could be obliging to adjust the required thermo optical properties for temperature stabilization of the external spacecraft's surfaces.

References

Abdel-Aziz, Yehia A., Abd El-Hameed, Afaf M., El-Tokhy, Fatma S., Ahmed Ghitas, Selim, I., and Sabry, M., 2013, Ground-Based simulation for the Effects of Space Plasma on Spacecraft, Advances in Space Research Journal, Elsevier Pub., 51, 133–142.

Abd El-Hameed, Afaf M., Sabry, M., Ahmed Ghitas, El-Tokhy, Fatma S., and Schlosser, V., 2015, Effects of LEO Plasma Exposure on the Performance of Silicon Solar Cells, J. of Electronic Materials, Springer, 44, 12, 4740.

Abd El-Hameed, Afaf M., Abdel-Aziz, Yehia A., and El-Tokhy, Fatma S., 2017, Anodic Coating Characteristics of Different Aluminum Alloys for Spacecraft Materials Applications, J. of Materials Sciences and Applications (MSA), 8, 2, 197-208.

Akitoshi Takahashi, Ryo Muraguchi, Minoru Iwata, and Mengu Cho, 2014, Charging and Arcing Test on Semi-Conductive Coated Solar Coupon Panel, IEEE Transactions on Plasma Science 42(2):384-390.

Arifur R. Khan, Wu Jiang, Kazuhiro Toyoda, and Mengu Cho, 2013 Electron and proton irradiation effect on bulk resistivity of polyimide measured in vacuum, 57th Space Science and Technology Conference, JSASS-2013-4637.

Ferguson, D.C., 1991, Proceedings of the 10th Space Photovoltaic Research and Technology Conference, NASA LeRC, May 7-9, 1991, Invited Paper. "LEO Space Plasma Interactions." NASA CP 3121.

Fukuda, Hiroshi, Toyoda, Kazuhiro, and Cho, Mengu, 2017, Mission Results Analysis of High-Voltage Technology Demonstration Satellite HORYU-II, IEEE Transactions on Plasma Science PP (99), 1-9 · DOI: 10.1109/TPS.2017.2705726.

Galofaro J.T., Doreswamy C.V., Vayner B.V., Snyder D.B., and Ferguson D.C., 1998, Ground Based Vacuum Tests of Electrical Breakdown on an Anodize Aluminum Plate Immersed in Low Density Plasma, Copyright© 1998, American Institute of Aeronautics and Astronautics, Inc.

Galofaro J.T., Doreswamy C.V., Vayner B.V., Snyder D.B., and Ferguson D.C., 1999, Electrical Breakdown of Anodized Structures in a Low Earth Orbital Environment, J. Spacecraft and Rockets, 36, 4, 579-585.

Hillard G.B., and Ferguson D.C., 1995, Measured Rate of Arcing From an Anodized Sample on the SAMPIE Flight Experiment, 33rd Aerospace Sciences Meeting & exhibit, AIAA 95- 0487.

Hillard, G.B. Bailey S.G., and Ferguson D.C., 2000, Anodized Aluminum as Used for Exterior Spacecraft Dielectrics, 6th Spacecraft Charging Technology Conference, AFRL-VS-TR-20001578, 1 September.

Hillard, G.B., Vayner, B.V., 2005, pacecraft charging effects on anodized aluminum surfaces. In: Energy Conversion Engineering Conference and Exhibit, (IECEC) 35th Intersociety,1, 63–68.

Hirokazu Tahara, Takahisa Masuyama, and Kouji Horikawa, 2006,"Ground-Based Experiment of Electric Breakdown of Spacecraft Insulator Surface in Ambient Plasma Environment", IEEE Transactions on Plasma Science · November 2006.

Jongeward, G., Katz, I., 1998, Effect of conduction and ion current on solar array arc thresholds. In: Proceedings of the 6th Spacecraft Charging Technology Conference, Hanscom AFB, MA, 297–301.

Leung, P., 1989, the Electrical Conductivity of ZOT after a Long Term Exposure to Thermal Vacuum Environment, Proceedings of Spacecraft Charging Technology Conference, 166-173.

Masahito Tagawa, Kumiko Yokota, Mengu Cho, and Hiroyuki Shimamura , 2010, A Consideration of Future Flight Material Exposure Experiments in Japan: Advanced Material Exposure Test Working Group's Proposal, Transactions of the Japan Society for Aeronautical and Space Sciences, Aerospace Technology Japan 8 (27).

Mengu Cho, 2007, Charging and Discharge in Vacuum and Space, IEEE International Vacuum Electronics Conference, IVEC '07, DOI: 10.1109/IVELEC.2007.4283197.

Robinson, P., and Whittlesey, A., 1980, Electrostatic Charging Characteristics of Thermal Control Paints as a Function of Temperature, Proceedings of Space Charging Technology, NASA CP-2182, Nov 12-14, 309-319.

S. B. Gupta, K. R. Kalaria, Naresh Kumar Parshottambhai Vaghela, S. Mukherjee, Rashmi S. Joshi, Suresh Edekkepravan Puthanveettil, Muthusamy Shankaran, Ranganath S. Ekkundi, 2014,

An Overview of Spacecraft Charging Research in India: Spacecraft Plasma Interaction Experiments-SPIX-II, IEEE Transactions on Plasma Science, 42(4):1072-1077.

Suryakant B. Gupta, Keena R. Kalaria, Naresh P. Vaghela, Rashmi S. Joshi1, , S. Mukherjee1, G. Usha, Joseph Thomas, R. Nukaraju, B. R.Uma, B. K. Muktha, G. Krishna Priya, Suresh E.Puthanveettil and M.Sankaran, 2016, Ongoing spacecraft charging research in India - Spacecraft Plasma Interaction eXperiments (SPIX-II) and the way forward, Spacecraft Charging Technology Conference 04 - 08 April 2016, ESA/ESTEC, Netherland.

Tahara H., Zhang L., Hiramatsu M., Yasui T., Yoshikawa T., Setsuhara Y., and Miyake S., 1995, Exposure of Space Material Insulators to Energetic Ions, J. Appl. Phys., 78, 6, 3719-3723.

Tahara H., Kawabata K., Zhang L., Yasui T., and Yoshikawa T., 1997, Exposure of Spacecraft Polymers to Energetic Ions, Electrons and Ultraviolet Light," Nucl. Instrum. & Methods, B121, 446-449.

Takahisa Masuyama, Masato Nagata, Tatsuo Onishi, Hirokazu Tahara, and Takao Yoshikawa, 2003, Ground Experiment and Numerical Simulation of Spacecraft Arcing in Ambient Plasma Environments, 8th Spacecraft Charging Technology Conference, NASA Marshall Space Flight Center, Oct. 20-23.

Teichman, L.A., 1989, NASA/SDIO, Space Environmental Effects on Material, Workshop, NASA- CP-3035.

Todd A. Schneider, M. Ralph Carruth, Jr., Miria M. Finckenor, Jason A. Vaughn, John Heard, and Dale Ferguson, 2001, An Experimental Investigation of the Effects of Charging on the International Space Station, Spacecraft Charging Technology, Proceedings of the Seventh 7th International Conference, 23-27 April, at ESTEC, Noordwijk, the Netherlands. Edited by R.A. Harris, European Space Agency, ESA SP-476, 405.

Tribble A.C., Lukins R., Watts E., Borisov V.A., Demidov S.A., Denisenko, V.A.Gorodetskiy A. A. Grishin, V.K., Nauma S.F., Sergeev V.K., and Sokolova S.P., 1996, United States and Russian Thermal Control Coating Results in Low Earth Orbit," J. Spacecraft & Rockets, 33, 1,160-166.

Tyler P. Black, Todd A. Schneider, Jason A. Vaughn, Blake R. Tiepel, Leonard Kramer and Philip L. Leung., 2006, Plasma-Induced Dielectric Breakdown of Anodized Aluminum Surfaces, 44th AIAA Aerospace Sciences Meeting 9-12 Jan., Reno, Nevada.

Zhang L., Yasui T., Tahara H., and Yoshikawa T., 1997, X-ray Photoelectron Spectroscopy Study of the Interactions of O+ and N+ Ions with Polyimide Films, Jpn., J. Appl. Phys., 36, 8, 5268-5274.